JASA ARTICLE

Holey-structured tungsten metamaterials for broadband ultrasonic sub-wavelength imaging in water

Lorenzo Astolfi,[1] David A. Hutchins,[1,a)] Peter J. Thomas,[1] Richard L. Watson,[1] Luzhen Nie,[2] Steven Freear,[2] Adam T. Clare,[3] Marco Ricci,[4] and Stefano Laureti[4]

[1]*School of Engineering, University of Warwick, Coventry CV4 7AL, United Kingdom*

[2]*School of Electronic and Electrical Engineering, University of Leeds, Leeds LS2 9JT, United Kingdom*

[3]*Department of Mechanical, Material and Manufacturing Engineering, University of Nottingham, University Park, Nottingham NG7 2RD, United Kingdom*

[4]*Department of Informatics, Modelling, Electronics and System Engineering, University of Calabria, 87036 Rende, Italy*

ABSTRACT:

Metamaterials exhibiting Fabry–Pérot resonances are shown to achieve ultrasonic imaging of a sub-wavelength aperture in water immersion across a broad bandwidth. Holey-structured metamaterials of different thickness were additively manufactured using a tungsten substrate and selective laser melting, tungsten being chosen so as to create a significant acoustic impedance mismatch with water. Both broadband metamaterial behavior and sub-wavelength imaging in water are demonstrated experimentally and validated with finite element simulations over the 200–300 kHz range.

© 2021 Author(s). All article content, except where otherwise noted, is licensed under a Creative Commons Attribution (CC BY) license (http://creativecommons.org/licenses/by/4.0/). https://doi.org/10.1121/10.0005483

(Received 17 March 2021; revised 19 May 2021; accepted 8 June 2021; published online 7 July 2021)

[Editor: Richard Daniel Costley] Pages: 74–81

I. INTRODUCTION

Sub-wavelength acoustic imaging is possible within the near field of an object, provided the evanescent component of the scattered field, carrying details with high spatial frequency, can be recovered via Fabry–Pérot (FP) resonances within a metamaterial structure.[1] The use of such holey-structured metamaterials has been demonstrated in air.[1–3] In some cases, enhancement of the evanescent wave magnitude has been reported as a consequence of highly anisotropic equi-frequency contours.[4] The latter magnification can also be achieved by using a membrane-based metamaterial with a negative effective density.[5] In the far field, imaging is conventionally diffraction-limited to half a wavelength. Several structures have been proposed for surpassing this limit in acoustics, including phononic crystals,[6,7] metamaterial-based two-dimensional (2D) hyperlenses,[8] and three-dimensional (3D) superlenses.[9]

Acoustic metamaterials are structures engineered to obtain exotic properties, such as extraordinary transmission,[10] absorption,[11] or sub-wavelength imaging.[9,12,13] Here, we are primarily interested in structures that contain arrays of periodic sub-wavelength holes, each of which acts as a Fabry–Pérot resonator. In the present case, these metamaterials take the form of metallic plates containing periodic arrays of sub-wavelength holes. Such structures were chosen as they can potentially exhibit sub-wavelength imaging properties over a range of frequencies. Figure 1 illustrates a typical structure, where the geometry is defined by the lattice parameter Λ (the distance between the centers of two neighbouring holes), this being the sum of the hole dimension a and wall thickness w. The channel depth is equivalent to the metamaterial sample thickness h.

The main acoustic transmission mechanism is via FP resonances within fluid-filled channels,[13] provided that the acoustic impedance of the solid matrix is high compared to that of the fluid within each hole.[1] These resonances will occur in metamaterial channels at frequencies that depend primarily on the metamaterial thickness h.[14] As long as the operating wavelength is much larger than the lattice parameter Λ, FP resonances couple with evanescent waves at the far side of the metamaterial, which is beneficial for sub-wavelength imaging.

The creation of FP resonances is enhanced when the metamaterial structure is fabricated from a solid material with an acoustic impedance Z that is very different from the surrounding medium, in our case water. This limits the transmission of acoustic signals into the solid structure, potentially avoiding complicated acoustic interactions. In air, this condition can be satisfied by many polymers and metals, since their impedance differs by several orders of magnitude from that of air.[1–3] Fewer experiments have been performed in water, mostly because of the lower impedance mismatch between water and commonly used materials, although an example of characterization of metallic components in water can be found in Ref. 12. Another example was presented in Ref. 15, where the concept of trapping air inside a polymer shell was exploited to build metamaterials for sub-wavelength imaging in water. Here, we address the

a)Electronic mail: d.a.hutchins@warwick.ac.uk

 ©Author(s) 2021.

https://doi.org/10.1121/10.0005483

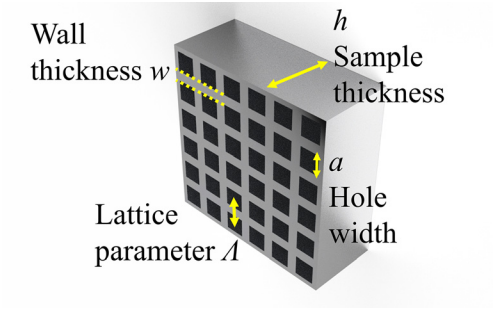

FIG. 1. (Color online) Schematic diagram of a holey metamaterial defined by Λ, a, w, and h.

design and fabrication of metallic holey-structured metamaterials displaying broadband ultrasonic behavior and sub-wavelength imaging in water.

A simple analysis of a single hole in a structure with an infinite impedance mismatch with water would expect FP resonances at frequencies f_n of

$$f_n = n\,\frac{c}{2\,h}, \tag{1}$$

where n is a positive integer representing the harmonic number, c is the speed of sound in water (1480 m·s^{-1}), and h is the metamaterial thickness (the channel length). However, to obtain the effective resonant frequency, open-ended pipe lengths have to be corrected by a factor Δl (Ref. 16), given by

$$\Delta l = 0.66\,a, \tag{2}$$

where a is the hole width. This factor has then to be added to the hole depth h to get the effective "pipe" length h_{eff}, given by

$$h_{eff} = h + \Delta l. \tag{3}$$

As will be described below, average hole widths of $a = 0.68$ mm were used experimentally. Thus, h_{eff} for an open-ended pipe in water with $h = 6$ mm and $a = 0.68$ mm is $h_{eff} = 6.45$ mm, expected to resonate at a frequency of 230 kHz.

When λ is much larger than both a and Λ, the presence of resonant standing waves leads to a prediction of a transmission coefficient that is unity for both propagating and evanescent waves in the perfect case of plane waves at normal incidence. Under these conditions, an object could be imaged at wavelengths below the diffraction limit. However, for this to happen, the metamaterial has to be placed close to the object being imaged. This is because the evanescent wave amplitude decreases exponentially with distance from the metamaterial surface, being effectively too low at distances beyond a wavelength. At resonance, imaging resolution is dictated by both the hole size a and the spacing between the channels within the metamaterial, as defined by the lattice parameter Λ.[1] It is thus beneficial to have small holes that are as closely spaced as possible.

One of the practical limits in this regard is the finite tolerance and precision of manufacturing methods for metallic components, which often depend on the aspect ratio of the holes in a FP material. Additive manufacturing was chosen in the present case, and a review of additive manufacturing methods for fabricating metamaterials can be found in Ref. 17. Note that, in addition to the expected surface roughness effect on acoustic behavior following fabrication, the presence of the no-slip condition near the hole walls might introduce a very small change in resonance frequency as a consequence of the sound velocity gradient.[18]

The present work demonstrates that metallic FP-based holey metamaterials can be designed and manufactured so as to operate at ultrasonic frequencies in water over the 200–300 kHz range. This paper describes the effect of sample thickness h of holey metamaterials in the generation of FP resonances and subsequent transmission of acoustic energy in water immersion. Sub-wavelength imaging is then made possible by the interaction between acoustic signals emitted by each of the holes in the structure. Finite element simulations have been performed to predict the formation of the expected FP resonances and the resulting imaging performance, and the predictions were compared to experimental results. The aim is to demonstrate that individual well-designed metallic metamaterials can be used to record images with sub-wavelength features across a range of frequencies.

II. SAMPLE FABRICATION AND EXPERIMENTAL ARRANGEMENT

The experiments in this study were performed in the 200–300 kHz ultrasonic frequency range, where the wavelength of ultrasound in water (λ_w) ranges from 4.9 to 7.4 mm. It was thus important that the hole size (a) and lattice parameter (Λ) spacing in the metamaterial samples were sufficiently small to ensure metamaterial behavior. It was also important that the acoustic impedance (Z) of the material was as high as possible, for the reasons outlined earlier. Tungsten was chosen in our experiments, due to its high value (Z_T) compared to water (Z_W) so that $Z/Z_W = 67.8$. This arises mainly from its high density (see Table I for details and a comparison to water).

Tungsten metamaterial samples were designed for a nominal hole size of $a = 0.68$ mm. These were fabricated by WOLFMET Ltd. (Manchester, UK), using selective laser melting (SLM), an additive manufacturing technique. As stated above, sub-wavelength imaging is made possible by resonances within a set of closely spaced channels whose

TABLE I. Speed of sound, density and acoustic impedance for water and tungsten used in the models.

Material	Longitudinal speed of sound m·s^{-1}	Density kg·m^{-3}	Acoustic impedance (Rayls × 10^6)
Water	1480	1000	1.48
Tungsten	5200	19 300	100.4

size and spacing need to be much smaller than the wavelength of the acoustic signal. In our case, the choice of square holes maximizes the area taken up by the holes, while allowing thin metal walls (note that conventional machining would find such structures difficult to build). Note that this hole size is close to the limit of resolution for tungsten structures printed using current SLM techniques. Two samples were fabricated with sample thicknesses of $h = 3$ mm and $h = 6$ mm. Photomicrographs of a typical structure are shown in Fig. 2, with this particular sample having 24 holes, with $a = 0.68$ mm separated by a 0.52 mm wall thickness so that $\Lambda = 1.2$ mm. These samples allowed the effect of sample thickness (h) to be explored for the smallest hole size that could be fabricated reliably using SLM. It was estimated that the average superficial roughness parameter R_a, which affects the roughness of the internal channel structure, was $R_a = 46.75\ \mu$m. This was measured using a Contour GT-K interferometer (Bruker Corp., Billerica, MA). Note that these values were expected from the estimated resolution limits of the SLM process.[19]

The experiments were performed within a $400 \times 350 \times 200\ \text{mm}^3$ water tank. A National Instruments (Austin, TX) PXI 5421 waveform generator created linear chirp signals, which were then amplified before being used to excite a 22 mm diameter piezocomposite ultrasonic transducer with a center frequency of 300 kHz (Cambridge Tech Ltd., Cambridge, UK). The source was placed at a distance of 140 mm from the front surface of both the $h = 3$ and $h = 6$ mm thick metamaterial samples. The aim of the first experiment was to measure the transmission response of the tungsten metamaterials in through transmission. The transmitted pressure field was detected using a 0.2 mm diameter hydrophone (Precision Acoustics, Dorchester, UK) with the hydrophone being able to be scanned along three axes using a custom-built 3D motor-controlled scanning system. A National Instruments PXI 5122 digitizer was used to acquire the 16 bit signal at 100 megasamples (MS)/s sampling frequency. Each acquired signal was recorded as a time waveform but also transformed into the frequency domain using a chirp z-transform (CZT) algorithm (a generalization of the discrete Fourier transform). CZT was preferred over the FFT because it is possible to tailor the frequency resolution by changing start and stop frequencies and the number of output samples required. For further information about the CZT, the reader is referred to Ref. 20.

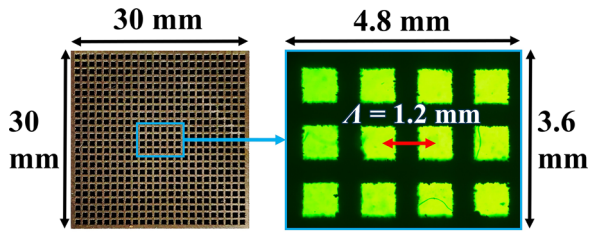

FIG. 2. (Color online) Image of a tungsten metamaterial sample with $a = 0.68$ mm and $\Lambda = 1.2$ mm. An expanded micrograph of the area indicated illustrates the effect of surface roughness.

III. RESULTS

A. Finite element simulations

COMSOL Multiphysics® (COMSOL, Stockholm, Sweden) was first used to model a plane incident pressure wave irradiating a single-hole structure within water. An absorbing boundary was used to simulate anechoic conditions to avoid reflections. A tetrahedral mesh was used so as to have 10 elements per side in each of the channels. In this model, the block was assumed to be an ideal material whose acoustic impedance differs from that of water by several orders of magnitude (as in the case of tungsten), so as to approximate a hard boundary. The frequency response was then predicted as the absolute pressure in the channel at discrete frequencies. The FE model assumed that water could be represented by an ideal fluid, which means that the liquid was assumed to be inviscid. Hence, although the no-slip condition was not satisfied in the modeling, this was considered to be a valid approach, as this condition is expected to be a negligible factor in water over the frequency range considered here.[18]

Figure 3(a) shows the geometry adopted for the single-channel model, and Fig. 3(b) shows the predictions obtained for a single-channel hole of width $a = 0.68$ mm for $h = 3$ mm and $h = 6$ mm, respectively. For $h = 3$ mm [Fig. 3(b)], it is evident that a single FP peak is predicted to occur at a frequency of 208 kHz. This is slightly different from that expected from Eqs. (1)–(3), which predicts a value of 215 kHz for the hole size of $a = 0.68$ mm. For $h = 6$ mm, however, three resonances are now visible. Equations

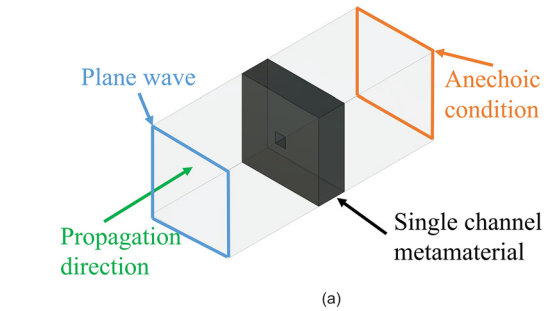

(a)

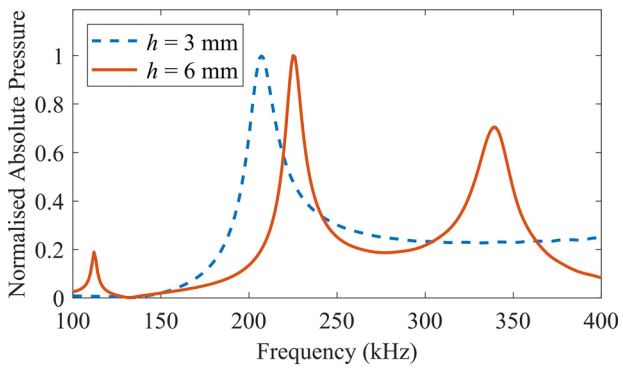

(b)

FIG. 3. (Color online) (a) Geometry of the 3D single-channel model showing the incident wave direction. (b) The simulated absolute value of pressure for $h = 3$ mm and $h = 6$ mm, showing clear FP peaks.

https://doi.org/10.1121/10.0005483

(1)–(3) predict these resonant frequencies to be 115, 230, and 345 kHz, respectively, whereas their values predicted by modeling are 113, 226, and 339 kHz. Thus, in both cases, there only exist minor differences between COMSOL model predictions and simple analytical theory. It can be seen in Fig. 3(b) that the single-channel model for $h = 6$ mm is nearer to the predicted theory than its 3 mm equivalent. This is thought to be due to the higher aspect ratio (width to length) of each channel, noting that thicker metamaterials create better resonances (but in practice will be more difficult to fabricate due to the need to create longer, thinner holes). In fact, small deviations of FP resonance frequencies from the ideal case might be expected, as such a phenomenon has already been seen in optics. Here, experiments with optical gratings observed a deviation of up to 16% in some cases.[21]

The $h = 3$ mm thick channel resonates at 208 kHz as its first harmonic. The responses of Fig. 3(a) were obtained at the channel halfway point (1.5 mm). Conversely, the $h = 6$ mm channel also generated a second harmonic creating standing waves at one-third (2 mm) and two-thirds (4 mm) of the channel length at 226 kHz. If probed at 3 mm, the second harmonic would not be visible, as it is the middle point between the standing waves generated by the second harmonic. Hence, the pressure was probed at 1/4 of the distance into the channel, at a distance of 1.5 mm, so that all the harmonics could be represented at the same point.

Note that the present experiments were restricted to the 200–300 kHz frequency range, so as to be able to compare two different thicknesses of tungsten metamaterials across the same bandwidth. Thus, the response at the first harmonic resonant frequencies of the $h = 3$ mm samples could be compared to those arising from the second harmonic resonances of the $h = 6$ mm samples. It can be seen that the FP peaks in the 200–250 kHz range for the 3 and 6 mm thick metamaterials are not at the exact expected frequency, suggesting that the aspect ratios of the channels play a role in the generation of resonances.

Consider now a metamaterial containing a matrix of 5×5 holes, with $h = 6$ mm and $a = 0.68$ mm, as depicted in Fig. 4(a). The same model as was illustrated in Fig. 3(a) was employed, with the same mesh size and model volume, only now more holes were added. By calculating the frequency-dependent transmission as a ratio of total energy transmitted by all 25 channels at the outlet and dividing this by that present at the inlet, it can be seen that the resultant peak resonance response is shifted up slightly to 271 kHz when compared to a single hole, as illustrated in Fig. 4(b), but also that the response is now over a wider frequency range. This might be expected due to interactions between the acoustic fields emanating from multiple holes in patterned holey metamaterials, which will affect the frequency response of the overall structure. This suggests that such metamaterials can operate over a wider range of frequencies than might be expected if the resonance of a single hole only were considered. This is of substantial interest and relevance because a broad bandwidth is a highly desirable feature in acoustic imaging systems.

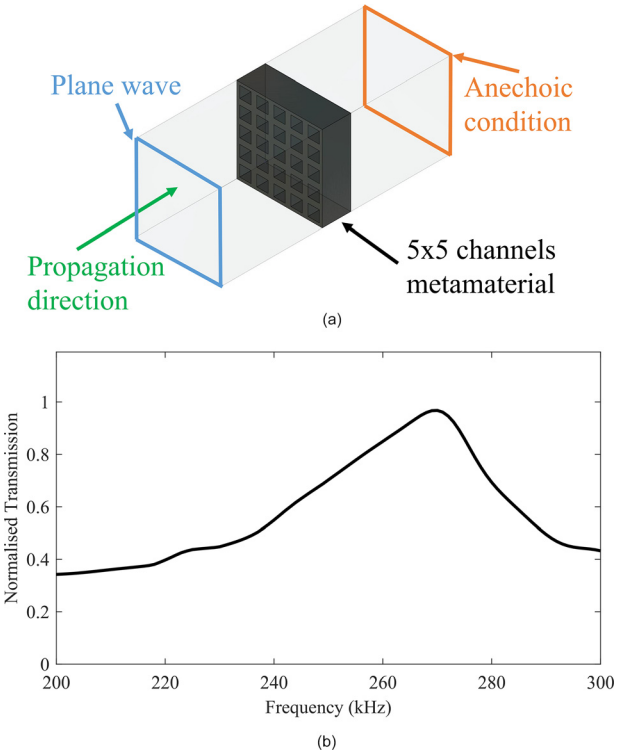

FIG. 4. (Color online) (a) Geometry of the 3D 5×5 channel model, showing the incident wave direction. (b) Simulated normalised transmission obtained as the ratio of transmitted energy over inlet energy as a function of frequency for a 5×5 metamaterial with $h = 6$ mm and $a = 0.68$ mm.

It was stated earlier that square holes were chosen to maximise cross-sectional hole areas. However, there are examples in the literature of both square[2] and circular[21] hole geometries exhibiting FP resonances. Our FE simulations indicate that square holes result in a sharper resonance, but at slightly higher frequencies than those for the equivalent size of circular holes. This further illustrates that square holes were a good choice for these metamaterials.

Simulations were also performed to examine the possible imaging capability of such metamaterial structures. To achieve this, a model was created to demonstrate that metamaterial designs considered in this work could be used to reconstruct an E-shaped aperture machined in a 1 mm thick brass plate. The aperture had a feature linewidth of only 1 mm, which corresponded to $\lambda/6$ at 245 kHz. The aperture dimensions are the same as those used in the experimental measurements described below.

The geometry used for the finite element (FE) model is shown in Fig. 5(a), with the E-shaped aperture in front of the metamaterial. Figures 5(b)–5(d) show the expected change in pressure amplitude across a plane parallel to the metamaterial output surface, at a small distance of 0.1 mm from it. This small distance is required to allow the interaction of evanescent waves to occur. Figure 5(b) shows the prediction obtained for $h = 3$ mm and $a = 0.68$ mm at 245 kHz, and Fig. 5(c) displays the result for the thicker metamaterial with $h = 6$ mm and $a = 0.68$ mm at 276 kHz. It is clear that the two metamaterials considered were able to

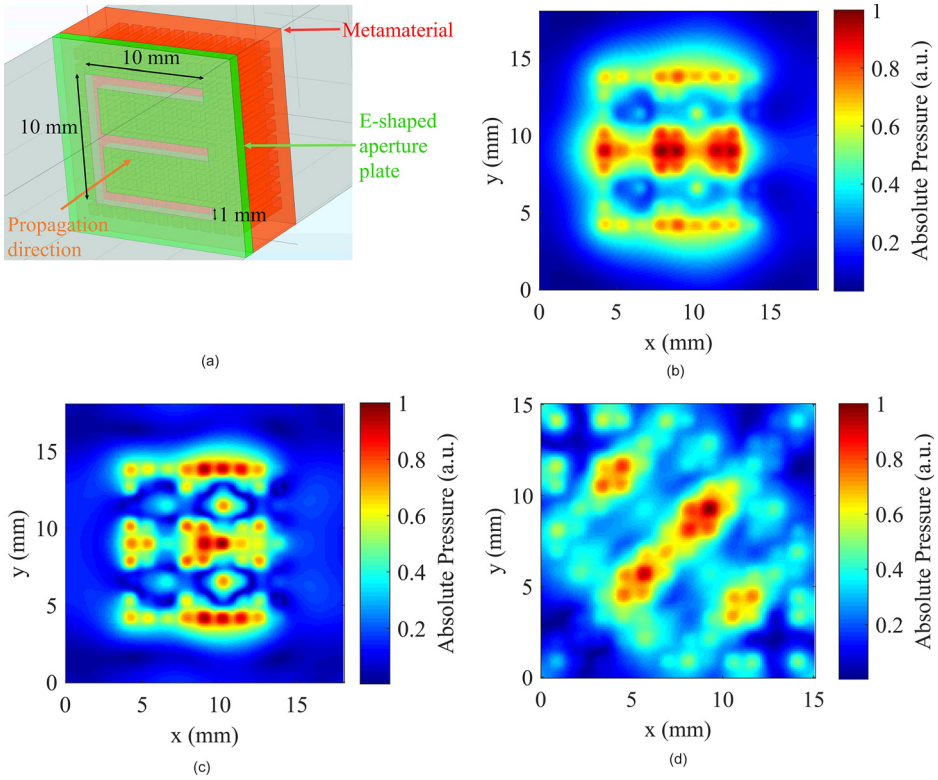

FIG. 5. (Color online) (a) Model adopted for imaging a sub-wavelength E-shaped aperture. (b)–(d) Simulated normalised pressure fields at 0.1 mm distance from the metamaterial's output plane. These were obtained for (b) $h = 3$ mm and $a = 0.68$ mm at 245 kHz, (c) $h = 6$ mm and $a = 0.68$ mm at 276 kHz, and (d) the same conditions as in (b) but with the aperture rotated by 45°.

resolve the E-shaped absolute pressure field. In all cases, the images show the output from individual holes as areas of higher amplitude, which interact to form the image of the E.

The simulation shown in Fig. 5(d) was performed to illustrate the case of an aperture rotated by 45° relative to the metamaterial ($h = 3$ mm) at 245 kHz. It can be seen that the vertical arm of the letter E is more clearly resolved, as is the whole object. This seems to indicate that orientation effects could be important where lattice parameters of the metamaterial are in the range studied here, where only a few holes are employed for imaging within the geometry of the aperture. However, it does illustrate that rotation has preserved the ability to retain sub-wavelength imaging.

B. Experimental imaging with metamaterials

To examine the metamaterial performance experimentally, measurements were taken both with and without the metamaterials in place. This allowed both the input pressure field and the output at the far side of the metamaterial to be recorded. The ratio of this output to that without the metamaterial in place was then used to determine the metamaterial response. By using a linear chirp excitation signal, a transmission coefficient curve could be calculated as the ratio of the magnitude of the CZT with the metamaterial in place with that of just water and then normalised. The lateral dimensions of the tungsten metamaterial samples were 30 mm × 30 mm, each containing an array of 24 × 24 holes. To approximate the incident wave generated by a 22 mm diameter source to a plane wave, only the inner 10 mm × 10 mm surface was considered. The distance between ultrasonic source and metamaterial was 140 mm, while the hydrophone was scanned as close to the far side of the metamaterial as possible, at a distance of 0.5 mm. Figure 6 shows an example of the transmission curve obtained with a hydrophone measurement averaged over the surface of 100 mm^2 for $h = 6$ mm and $a = 0.68$ mm, where a comparison is given to the simulated response of Fig. 5.

It can be seen that both the experimental values and those predicted by the COMSOL model are broadband. Experimentally, the bandwidth could have been broadened due to the surface roughness and non-square cross section of the channels (see Fig. 2) resulting from the SLM fabrication process. This would cause an increase in scattering, reducing the quality factor Q of the resonance and increasing bandwidth. This broadening of the range of operation is

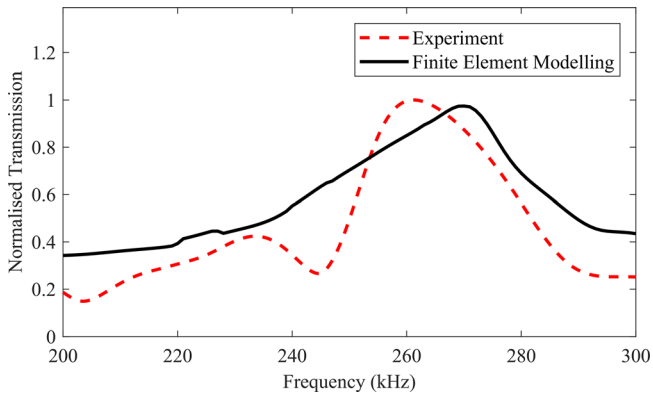

FIG. 6. (Color online) Experimental results (solid line) for the transmission spectrum obtained for a tungsten metamaterial with $h = 6$ mm and $a = 0.68$ mm.

https://doi.org/10.1121/10.0005483

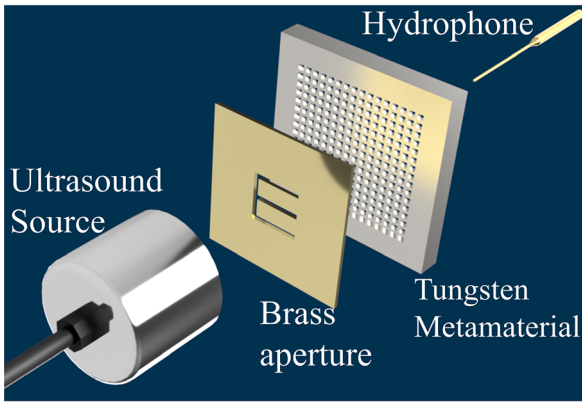

FIG. 7. (Color online) Experimental arrangement used to study imaging of an aperture in through-transmission. The 22 mm diameter ultrasound source was located at a distance of 140 mm from the aperture. The aperture and measurement hydrophone were both 0.5 mm from the respective surface of the metamaterial.

likely to be beneficial if broad bandwidth imaging is required (e.g., so as to implement certain signal processing strategies).

Once FP resonances were confirmed, a second experiment was performed to demonstrate the imaging properties of these metamaterials. The E-shaped aperture shown earlier in Fig. 5(a) was placed at a distance of 0.5 mm from the input surface of the metamaterial and parallel to it. It would be expected that the pressure field coming from the aperture would be transferred efficiently through the metamaterial because of the coupling of FP resonances with evanescent waves. This second experiment used a 75 μs long linear chirp signal swept from 100 to 400 kHz, allowing a range of frequencies to be explored efficiently. This excited the 22 mm diameter ultrasonic source, which was at a distance of 140 mm from the aperture (see Fig. 7). Each segment of the E aperture was 10 mm long and 1 mm wide, the latter dimension corresponding to $\sim\lambda/6$ at 245 kHz in water; this would be below the expected diffraction limit obtainable from conventional imaging. The magnitude of the signal scanned by the hydrophone was recorded in each location across a 2D plane parallel to the sample, at a distance of 0.5 mm from the far surface. Each metamaterial was scanned in a 131 × 131 grid of points, using a 0.14 mm step size at a plane 0.5 mm from the output surface of the metamaterial. The area covered by each scan was thus ~18 mm × 18 mm.

The results of these imaging experiments are shown in Fig. 8. It can be seen that both metamaterial thicknesses have reconstructed the basic shape of the sub-wavelength object at the chosen frequencies of 245 kHz (for $h = 6$ mm) and 276 kHz (for $h = 3$ mm). In this case, the shape of the image of the E aperture can be compared to that of the simulation in Fig. 5. In both cases, the shape of the letter can be clearly identified.

The experimental results are consistent with the FE predictions of Fig. 5, in that both thicknesses of the metamaterial design were able to recover the pressure field, employing the same frequencies as the numerical simulation. Details of the images differ; note that the presence of holes in the metamaterial structure was more obvious for $h = 6$ mm at 245 kHz but that signal levels were higher for the thinner $h = 3$ mm structure at a slightly higher frequency. This latter effect could be due to the fact that a thin metamaterial would be expected to experience less loss due to surface roughness effects with each hole. Imaging resolution could also have been affected due to experimental factors such as misalignment, small changes in hole shapes, roughness between samples, etc. However, it remains the case for a particular metamaterial structural design in terms of hole shape, size, and spacing that the quality of each image will be mainly dictated by the metamaterial thickness and the differences in amplitude between one harmonic and the next.

The experimental bandwidth of the response shown earlier in Fig. 6 illustrates that in our experiments, the material was operating across a broad range of frequencies. To illustrate this, Figs. 9(a) and 9(b) show experimental results obtained at four different frequencies for both thicknesses of metamaterial ($h = 6$ mm and $h = 3$ mm). It can be seen that the quality of the resultant image varies with frequency but that better results were observed in the 265–285 kHz range in both cases and that the 6 mm thick metamaterial seemed to be better reconstructing the object. This demonstrates that images could be reconstructed across a 60 kHz frequency range. Thus, while the modeling results for a single channel would predict the best response at 208 and 226 kHz, experiments and simulations for metamaterials with mutiple holes

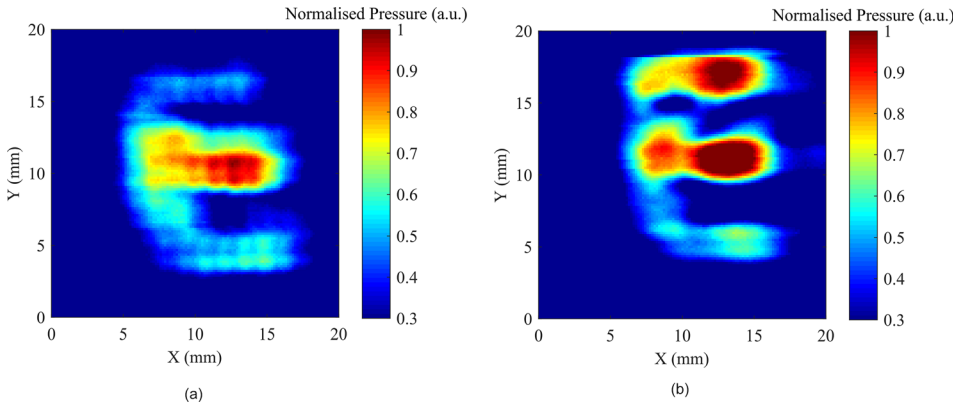

FIG. 8. (Color online) Experimental absolute pressure fields detected and after transmission through the metamaterial with $a = 0.68$ mm. (a) $h = 6$ mm at 245 kHz; (b) $h = 3$ mm at 276 kHz.

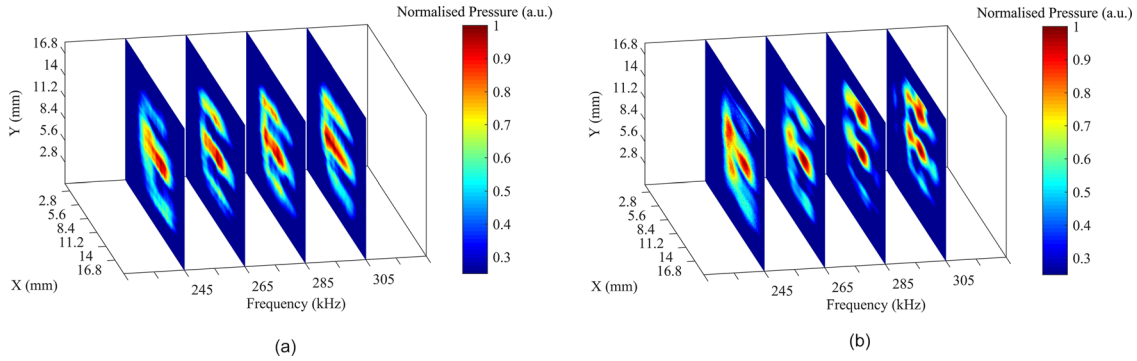

FIG. 9. (Color online) Experimental results for the normalised pressure fields at a range of frequencies between 245 and 305 kHz. These were obtained for (a) $h = 6$ mm and (b) $h = 3$ mm.

are seen to shift this response upward in frequency and to broaden the bandwidth. Additive manufacturing imperfections in hole geometry may also be responsible for broadening the operational range at ultrasonic frequencies, and this could be a useful feature in future designs of such metamaterials.

To further confirm the collimation effect in water, the imaging experiment of Fig. 9 was repeated but now in the absence of a metamaterial. In this way, the transmitted field both with and without the metamaterial in place could be compared. The results are shown in Fig. 10. This illustrates that, without the metamaterial in place, the E-shaped aperture was not resolved clearly. Further, a comparison of Figs. 9 and 10 demonstrates the effectiveness of the metamaterial in capturing the details of the aperture, which was not possible without it.

IV. CONCLUSIONS

It has been demonstrated that additively manufactured tungsten metamaterials can be used to image objects with a size down to $\lambda/6$ at ultrasonic frequencies in water. The experimental results agree with the trends seen in FE modeling, and the metamaterial responses were demonstrated to be broadband. FP resonances were observed over a much wider range of frequencies when multiple holes interacted with evanescent waves. Such resonances were demonstrated both numerically and experimentally to lead to sub-wavelength imaging. Our studies show that additively manufactured tungsten metamaterials can achieve sub-wavelength imaging in water and that SLM is a suitable manufacturing technique to fabricate broadband metamaterials in the range of frequencies considered.

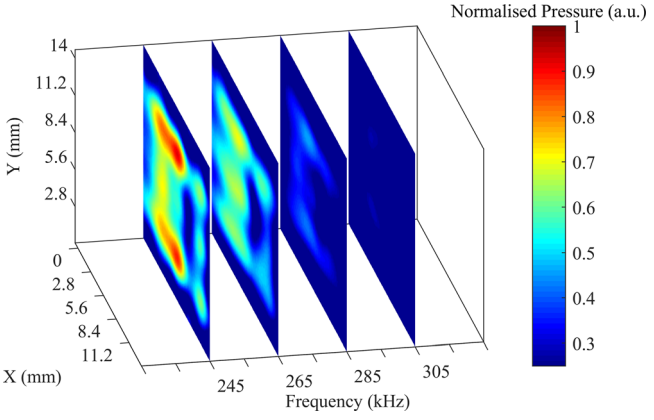

FIG. 10. (Color online) Experimental results for the normalised pressure field at a distance of 6 mm from the E-shaped aperture without a metamaterial being present. This is to allow a direct comparison with the results of Fig. 9.

ACKNOWLEDGMENTS

Funding for this work was provided through the UK Engineering and Physical Sciences Research Council (EPSRC), Grant Nos. EP/N034163/1, EP/N034201/1, and EP/N034813/1. The funding source had no involvement in collection, analysis, and interpretation of data.

[1]J. Zhu, J. Christensen, J. Jung, L. Martin-Moreno, X. Yin, L. Fok, X. Zhang, and F. J. Garcia-Vidal, "A holey-structured metamaterial for acoustic deep-subwavelength imaging," Nat. Phys. **7**(1), 52–55 (2011).
[2]S. Laureti, L. A. J. Davis, M. Ricci, and D. A. Hutchins, "The study of broadband acoustic metamaterials in air," in *Proceedings of the IEEE International Ultrasonics Symposium*, Chicago, IL (September 3–6, 2014), pp. 1344–1347.
[3]S. Laureti, D. Hutchins, L. Davis, S. Leigh, and M. Ricci, "High-resolution acoustic imaging at low frequencies using 3D-printed metamaterials," AIP Adv. **6**(12), 121701 (2016).
[4]Y. Cheng, C. Zhou, Q. Wei, D. Wu, and X. Liu, "Acoustic subwavelength imaging of subsurface objects with acoustic resonant metalens," Appl. Phys. Lett. **103**(22), 224104 (2013).
[5]J. J. Park, C. M. Park, K. J. B. Lee, and S. H. Lee, "Acoustic superlens using membrane-based metamaterials," Appl. Phys. Lett. **106**, 051901 (2015).
[6]S. Yang, J. H. Page, Z. Liu, M. L. Cowan, C. T. Chan, and P. Sheng, "Focusing of sound in a 3D phononic crystal," Phys. Rev. Lett. **93**(2), 024301–024301 (2004).
[7]J. H. Page, "Focusing of Ultrasonic Waves by Negative Refraction in Phononic Crystals," AIP Adv. **6**, 121606 (2016).
[8]J. Li, L. Fok, X. Yin, G. Bartal, and X. Zhang, "Experimental demonstration of an acoustic magnifying hyperlens," Nat. Mater. **8**, 931–934 (2009).
[9]X. Zhang and Z. Liu, "Superlenses to overcome the diffraction limit," Nat. Mater. **7**(6), 435–441 (2008).
[10]Y. Li, B. Liang, X. Y. Zou, and J. C. Cheng, "Extraordinary acoustic transmission through ultrathin acoustic metamaterials by coiling up space," Appl. Phys. Lett. **103**(6), 063509 (2013).
[11]H. Estrada, P. Candelas, A. Uris, F. Belmar, F. J. García De Abajo, and F. Meseguer, "Extraordinary sound screening in perforated plates," Phys. Rev. Lett. **101**(8), 084302 (2008).

[12]K. K. Amireddy, K. Balasubramaniam, and P. Rajagopal, "Holey-structured metamaterial lens for subwavelength resolution in ultrasonic characterization of metallic components," Appl. Phys. Lett. **108**(22), 224101 (2016).
[13]J. Christensen, L. Martín-Moreno, and F. J. García-Vidal, "Enhanced acoustical transmission and beaming effect through a single aperture," Phys. Rev. B Condens. Matter Mater. Phys. **81**(17), 174104 (2010).
[14]J. Christensen, L. Martin-Moreno, and F. J. Garcia-Vidal, "Theory of resonant acoustic transmission through subwavelength apertures," Phys. Rev. Lett. **101**(1), 2–5 (2008).
[15]S. Laureti, D. A. Hutchins, L. Astolfi, R. L. Watson, P. J. Thomas, P. Burrascano, L. Nie, S. Freear, M. Askari, A. T. Clare, and M. Ricci, "Trapped air metamaterials for ultrasonic sub-wavelength imaging in water," Sci. Rep. **10**, 10601 (2020).
[16]T. Boelkes and I. Hoffmann, "Pipe diameter and end correction of a resonant standing wave," Int. School Bangkok J. Phys. **5**, 1–3 (2011).
[17]M. Askari, D. A. Hutchins, P. J. Thomas, L. Astolfi, R. L. Watson, M. Abdi, M. Ricci, S. Laureti, L. Nie, S. Freear, R. Wildman, C. Tuck, M. Clarke, E. Woods, and A. T. Clare, "Additive manufacturing of metamaterials: A review," Addit. Manuf. **36**, 101562 (2020).
[18]T. J. Graham, A. P. Hibbins, J. R. Sambles, and T. A. Starkey, "Underwater acoustic surface waves on a periodically perforated metal plate," J. Acoust. Soc. Am. **146**(6), 4569–4575 (2019).
[19]S. L. Campanelli, N. Contuzzi, A. Angelastro, and A. Domenico, "Capabilities and performances of the selective laser melting process," in *New Trends in Technologies: Devices, Computer, Communication and Industrial Systems* (IntechOpen, London, UK, 2010).
[20]L. R. Rabiner and R. W. Schafer, "The chirp z-transform algorithm," IEEE Trans. Audio Electroacoust. **17**(2), 86–92 (1969).
[21]B. Hou, J. Mei, M. Ke, Z. Liu, J. Shi, and W. Wen, "Experimental determination for resonance-induced transmission of acoustic waves through subwavelength hole arrays," J. Appl. Phys. **104**(1), 014909 (2008).